

Efficiently-coupled microring circuit for on-chip cavity QED with trapped atoms

Tzu-Han Chang,¹ Xinchao Zhou,¹ Ming Zhu,¹ Brian M. Fields,¹ and Chen-Lung Hung^{1,2, a)}

¹⁾*Department of Physics and Astronomy, Purdue University, West Lafayette, IN 47907, USA*

²⁾*Purdue Quantum Science and Engineering Institute, Purdue University, West Lafayette, IN 47907, USA*

(Dated: 22 December 2024)

We present a complete fabrication study of an efficiently-coupled microring optical circuit tailored for cavity quantum electrodynamics (QED) with trapped atoms. The microring structures are fabricated on a transparent membrane with high in-vacuum fiber edge-coupling efficiency in a broad frequency band. In addition, a bus waveguide pulley coupler realizes critical coupling to the microrings at both of the cesium D-line frequencies, while high coupling efficiency is achieved at the cesium ‘magic’ wavelengths for creating a lattice of two-color evanescent field traps above a microring. The presented platform holds promises for realizing a robust atom-nanophotonics hybrid quantum device.

Cold atoms trapped and interfaced with light in photonic optical circuits form exciting hybrid quantum platforms for quantum optics and atomic physics. Strong optical confinement in nanophotonic waveguides or resonators greatly enhances atom-light coupling beyond those achieved in diffraction-limited optics, enabling new opportunities in studying light-matter interactions^{1–8} and radiative processes^{9–11}. On the circuit-level, nanophotonic engineering offers a variety of tools in modifying the photonic density of states^{12,13}, as well as controlling photon transport and device optical links^{14–18}, thus enriching the complexity of atom-photon interactions and quantum functionality. The indistinguishability and long coherence time of neutral atoms make an atom-nanophotonic hybrid platform inherently scalable, and by itself a strongly coupled many-body system^{13,19,20}. Recent developments in suspended photonic crystal waveguides and microring resonators^{8,21–24} hold great promises in realizing highly coherent quantum circuits with cold atoms in cavity QED and waveguide QED settings¹³.

Engineering an integrated photonic circuit that fulfills all technical requirements has so far remained a challenging task. Ideally, the circuit geometry should be compatible with atom cooling and trapping. Nanophotonic waveguides and resonators must be fabricated with high precision, and offer sufficient tunability for alignment with narrow atomic spectral lines. To perform quantum operations with high fidelity, photons should be coupled into and out of a circuit with high efficiency. It is advantageous that a photonic nanostructure could also be utilized to create far off-resonant optical traps to localize cold atoms^{25,26}. Taking cesium atoms for example, a two-color evanescent field trap formed using the ‘magic’ wavelengths ($\lambda_b \approx 794$ nm and $\lambda_r \approx 935$ nm) can create a better trap for coherent quantum operations^{27,28}. As such, all coupling elements to the circuit should work in a broad frequency band.

In the letter, we discuss design and full fabrication procedures of an efficiently-coupled microring optical circuit that meets all the requirements for building a robust hybrid quantum device. An overview of our platform is shown in Fig. 1,

where Si_3N_4 microring resonators are evanescently coupled to a bus waveguide in a pulley geometry for optical input and output [Fig. 1(b-c)]. The microrings are top vacuum-cladded and are fabricated on a transparent SiO_2 - Si_3N_4 double-layer membrane (Fig. 1(c) and Fig. 2), suspended over a large window (2 mm \times 8 mm) on a silicon chip. This ensures full optical access for laser cooling and cold atom trapping²⁹. The microring geometry is designed to optimize the cooperativity parameter $C = \frac{3\lambda^3}{4\pi^2} \frac{Q}{V_m}$ for cavity QED with cesium atoms²³, where $\lambda = \lambda_{D1} = 894$ nm ($\lambda_{D2} = 852$ nm) is the wavelength of Cs D1 (D2) line. The microring radius is $R \approx 15$ μm and the waveguide width and height are $(W, H) = (750, 380)$ nm, respectively (Fig. 2). A nearly optimal Q/V_m ratio is achieved, giving $C \approx 10 \sim 30$ with an intrinsic quality factor $Q \approx 1 \sim 3.3 \times 10^5$, currently limited by the surface scattering loss, and a mode volume $V_m \approx 500$ μm^3 , evaluated using the normalized transverse-magnetic (TM) mode field amplitude at an atomic position $z_t \approx 100$ nm centered above the microring dielectric surface. We adopt the fundamental TM-mode for its uniform polarization above a microring²³.

By lithographically scanning the length of each microring (Fig. 1(b)), their resonances approach the targeted frequency as shown in the transmission spectrum in Fig. 1(e). Precise alignment to the atomic spectral lines can be thermally tuned, for example, by a laser beam heating the silicon substrate under vacuum. The tunability is ~ 0.5 GHz/mW. The transmission spectrum is measured through lensed fibers coupled to either end of the bus waveguide via an edge-coupler (Fig. 1(d)). Each of the resonances in Fig. 1(e) displays nearly zero transmission $T \approx 0$, achieving the ideal critical coupling condition for probing atom-microring coupling; see Fig. 4.

We begin the circuit fabrication by preparing for a SiO_2 - Si_3N_4 double-layer membrane stack, deposited on a silicon wafer using low-pressure chemical vapor deposition (LPCVD) processes. For stable membrane release from the silicon substrate, the compressive stress of the SiO_2 layer (~ 2 μm thick) should be overcome by the tensile stress of the Si_3N_4 bottom-layer, giving a thickness-weighted tensile resulting stress³⁰. We arrive at a proper stress condition by post-annealing at around 1100°C for the Si_3N_4 bottom-layer and at 950°C after we deposited the SiO_2 layer, two hours for

^{a)}Electronic mail: clhung@purdue.edu

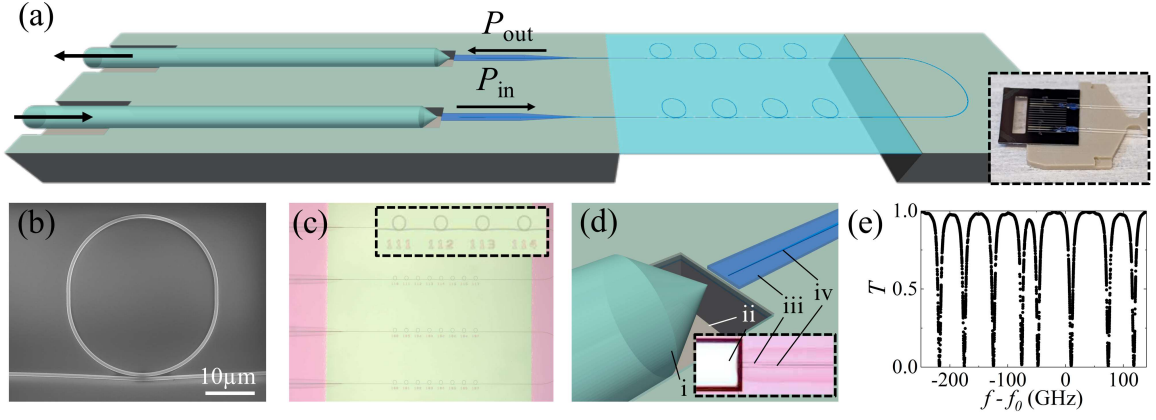


FIG. 1. (a) Schematics showing the microring resonators (b) on a transparent membrane, the coupling bus waveguide (c), and the top-cladded lens fiber edge-couplers (d) for optical input and output (arrows). The inset shows a fabricated circuit. (b) Scanning electron micrograph of a microring resonator and a bus waveguide in a pulley geometry. Short linear segments in the microring are added to fine-tune the resonator length. (c) Optical micrograph and a zoom-in view (inset) of the microring array. (d) Schematics and micrograph (inset) of the edge-coupler, displaying the lensed fiber (i), the U-shaped fiber groove (ii), and the HSQ top-cladding layer (iii) covering the tapered bus waveguide (iv). (e) Normalized bus waveguide transmission $T = P_{out}/P_{in}$ versus laser frequency f , showing multiple resonances each from a different microring; $f_0 = 335.116$ THz is near the Cs D1-line frequency.

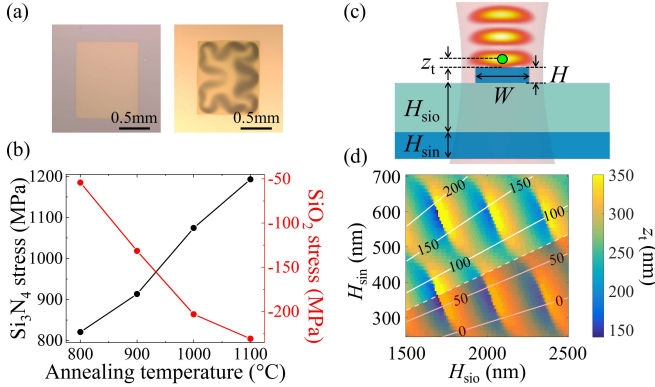


FIG. 2. (a) Optical micrographs of released membranes with tensile (left, 180 MPa) and compressive (right, -100 MPa) resulting stress. (b) Intrinsic stress of LPCVD Si_3N_4 and SiO_2 layers measured after post-annealing at various temperatures. (c) Illustration of a lattice of micro traps formed in a top-illuminating optical beam. Position z_t of the first trap center (green sphere) can be tuned by the layer thickness (H_{SiO_2} , H_{SiN}), as shown in (d). Solid lines indicate constant resulting stress (labeled in MPa) while shaded area marks the unstable region.

each time (Fig. 2(b)). In our results, a post-annealed membrane can be released free from buckling and severe cracking under a tensile stress of 70 ~ 180 MPa.

Optical reflectance is another crucial factor in determining the membrane thickness, primarily concerning atom trapping. For example, in a top-illuminating optical tweezer trap implemented in Ref.²⁹ or³¹, membrane reflection and interference result in a lattice of micro traps formed within a tweezer beam as shown in Fig. 2(c). We scan the $\text{SiO}_2/\text{Si}_3\text{N}_4$ layer thickness to minimize the position z_t of the first micro trap (formed by an anti-node) in a tweezer potential, while monitoring the resulting stress. An example is shown in Fig. 2(d), calculated for a $\lambda_r = 935$ nm tweezer trap focused by an objective of numerical

aperture N.A. = 0.35. A micro trap at $z_t \approx 150$ nm forms with layer thickness (H_{SiO_2} , H_{SiN}) $\approx (1.72, 0.55)$ μm within the stable membrane regime.

Once the membrane stack is fabricated, an additional LPCVD-grown Si_3N_4 top-layer is deposited, and the wafer is diced into centimeter-sized chips (Fig. 1(a) inset). Microring arrays and bus waveguides are then fabricated in the top layer using e-beam lithography with multipass writing and an inductively coupled plasma reactive-ion etching (ICP-RIE) process with CHF_3/O_2 gas chemistry³².

Either end of a bus waveguide is designed to taper down and terminate at a width of 70 nm for edge-coupling with a lensed fiber³³ (1 μm focused beam waist), which is placed inside a U-shaped fiber groove of ~ 65 μm depth (Fig. 1(d)). To achieve high coupling efficiency, a top-cladding structure on each edge-coupler is fabricated to improve symmetric mode matching with the lensed fiber. The geometry of the top-cladded edge-coupler has been numerically optimized using finite-different-time-domain calculations to achieve $\sim 70\%$ coupling efficiency at Cs D-lines. The same coupler yields an efficiency $\sim 70\%$ (60%) at $\lambda_r \approx 935$ nm ($\lambda_b \approx 794$ nm).

To fabricate the edge-coupler structures, we cover the tapered bus waveguides with ~ 1 μm -thick hydrogen silsesquioxane (HSQ) resist as the top-cladding material. Using second e-beam lithography, we define the top-cladding structures to inversely taper down along the bus waveguides (Fig. 1(d)) so to keep the microrings top vacuum-cladded. Fiber grooves and edge-coupler facets are defined in a subsequent photolithography step. HSQ and SiO_2 are then etched away in the ICP-RIE, followed by the Bosch process etching to create fiber U-grooves in the silicon.

The membrane is then released from the silicon substrate. A window at the backside of the chip is first defined using photolithography, while the front-side is protected with a thick layer of spin-coated photoresist (PMMA 950 coating with

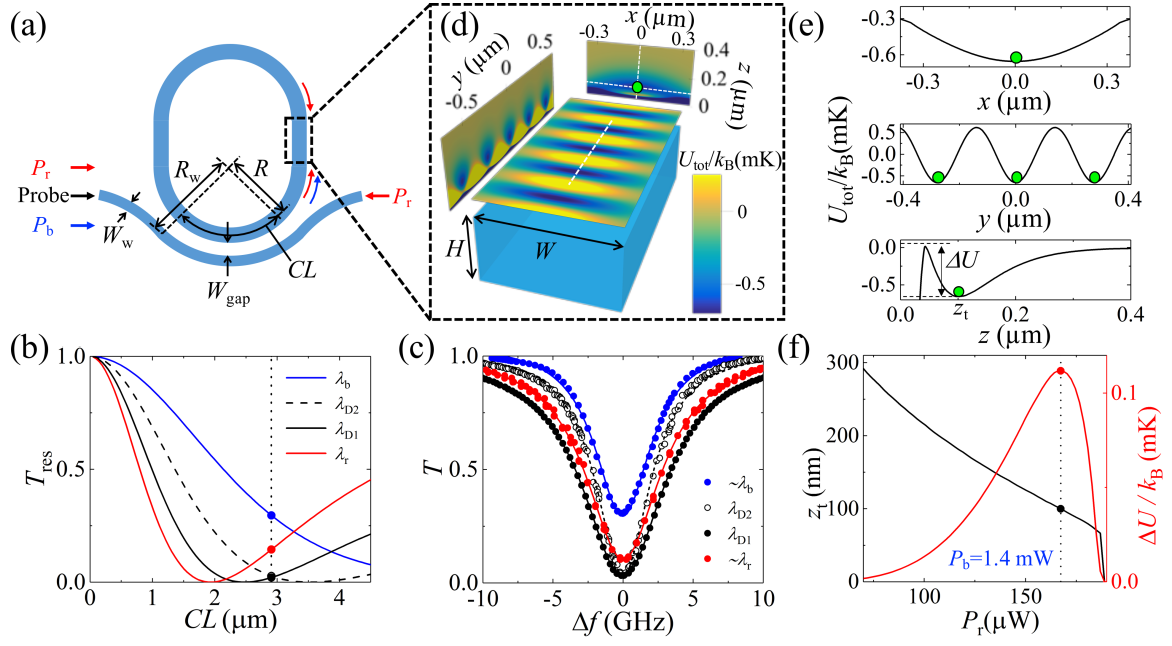


FIG. 3. (a) Schematics of the pulley-coupler. The coupler gap W_{gap} , bus waveguide width W_w , and bend radius R_w are optimized and fixed at $(0.21, 0.55, 15.86) \mu\text{m}$, respectively, along with the microring waveguide parameters $(W, H, R) = (0.75, 0.38, 15) \mu\text{m}$. CL is a variable coupling length. Color arrows depict the injected light for the two-color evanescent field trap (λ_b : blue, λ_r : red) and the atom probe ($\lambda_{D1, D2}$: black). (b) Simulated resonant transmission T_{res} versus coupling length CL at the indicated wavelengths. Vertical dashed line marks $CL = 2.9 \mu\text{m}$ for the fabricated device. (c) Measured transmission spectra (color symbols) with laser wavelengths as in (b). The spectra are shifted to display resonances at laser detuning $\Delta f = 0$, showing good agreement with calculation $T(0) \approx T_{\text{res}}$ (filled circles in (b)). Solid curves are fits to extract κ_c and κ_i . Based on these measurements, a two-color evanescent field trap can be accurately evaluated. (d) Potential cross sections above a linear segment of the microring (dashed box in (a)), calculated using injected power $(P_r, P_b) = (0.17, 1.4) \text{ mW}$, respectively. Potential line-cuts along the dashed lines are shown in (e). Green spheres mark the trap centers. (f) Variable vertical trap position z_t (black curve) and trap depth ΔU (red curve) as indicated in (e), adjusted through the power ratio P_r/P_b . Dashed line marks the condition at which $z_t = 100 \text{ nm}$.

Surpass 3000 adhesion promoter). Materials at the backside are etched away in the ICP-RIE and the Bosch process until leftover silicon is only $\sim 15 \mu\text{m}$ thick. To gently release the membrane, we perform wet-etching in a 12% aqueous TMAH solution at 65°C , followed by DI water rinsing and cleaning with PRS-2000 stripper and Nanostrip to expose the front-side photonic structures. Finally, a thin alumina layer ($\sim 5 \text{ nm}$) is deposited using atomic layer deposition to protect the microrings against cesium corrosion during experiments³⁴.

Our fabrication procedure yields nearly 100% success rate on membrane release. The released membrane is optically flat and has a root-mean-squared surface roughness of 1.4 nm . Additional chemical mechanical polishing step³² can be applied to the SiO_2 - Si_3N_4 double-layer stack following LPCVD. We have measured surface roughness down below 0.5 nm , which is expected to improve the microring quality factor to $Q > 10^6$ using similar fabrication procedures²³.

In the final step, optical lensed fibers are introduced to the fiber grooves. The alignment tolerance is $\sim \pm 0.3 \mu\text{m}$ for 1-dB excess loss. Fine adjustment in the U-groove is required prior to epoxy fixture. We note that misalignment can occur under vacuum when bulk epoxy outgases and shrinks. Therefore, only a thin layer of low viscosity UV epoxy (OG198-54) is applied for alignment fixture. We achieve $\sim 50\%$ ($\sim 3\text{dB}$ loss) coupling efficiency per facet, which persists under vacuum

pressure below 10^{-6} Torr. The fibers are guided out of a vacuum chamber without noticeable loss via a teflon feedthrough mounted on a Swagelok fitting³⁵.

We now discuss the design of pulley couplers (Fig. 3(a)), which allows us to separately optimize the bus waveguide parameters and the coupling length CL for efficient microring coupling over a wide frequency band. We perform a finite element method (FEM) analysis to calculate the microring coupling rate³⁶ $\kappa_c = |S \times \text{sinc}[(n_w R_w - nR) \frac{CL}{R\lambda}] \frac{CL}{R}|^2$, where $\text{sinc}(x) = \sin(\pi x)/\pi x$ is the normalized sinc function, λ is the coupling wavelength (ω is the angular frequency), $S = \frac{i\omega\epsilon_0}{4} \int (\epsilon_w(r, z) - 1) \tilde{\mathbf{E}}_w \cdot \tilde{\mathbf{E}}^* r dr dz$, and the integration runs over the cross-section of the bus waveguide with $\epsilon_w(r, z)$ being its dielectric function; $(\tilde{\mathbf{E}}_w, n_w, R_w)$ correspond to the normalized resonator (bus waveguide) mode field, the effective refractive index, and the bend radius, respectively. By comparing κ_c with the microring intrinsic decay rate κ_i , also evaluated using a FEM analysis²³, we can optimize the bus waveguide-microring coupling efficiency numerically.

Figure 3(b) shows the expected resonant transmission $T_{\text{res}} = |\frac{\kappa_i - \kappa_c}{\kappa_i + \kappa_c}|^2$ as a function of the coupling length CL . The better the coupling efficiency, the lower the transmission. Approaching the critical coupling condition ($\kappa_c = \kappa_i$), all of the resonant input photons can be drawn into the microring, hence, resulting in zero transmission $T_{\text{res}} =$

0. In this calculation, the pulley coupler geometry is chosen to improve the overlap of the critical coupling regions ($T_{\text{res}} \approx 0$) of all four relevant wavelengths. For the fabricated devices, we have selected $CL = 2.9 \mu\text{m}$ to approach critical coupling for Cs D-lines at λ_{D1} and λ_{D2} , respectively, while maintaining sufficient coupling efficiency near λ_b and λ_r magic wavelengths for two-color evanescent field traps²³. We anticipate $T_{\text{res}} = (0.02, 0.03, 0.14, 0.29)$ for test wavelengths $\lambda = (894, 852, 932, 795) \text{ nm}$, respectively, which are in very good agreement with the measurement $T(0) \approx (0.03, 0.04, 0.10, 0.31)$ as shown in Fig. 3 (c).

The agreement between the bus waveguide transmission measurement and full simulation results illustrate the fabrication precision of our microring optical circuit. Meanwhile, the absence of resonance splitting in the transmission data (Fig. 3 (c)) suggests that there is negligible mode-mixing caused by coherent back-scattering in the microring resonator^{23,37}. Therefore, the resonant TM modes preserve the traveling-wave characteristics of a whispering-gallery mode (WGM)²³.

Combining our measurement and FEM simulation results, we can now estimate the actual power required to create a stable two-color evanescent field trap. One sample scheme is illustrated in Fig. 3 (a). A resonant TM mode at wavelength λ_b is excited from the bus waveguide to create a smooth and short-range repulsive optical potential, preventing atoms from crashing onto the microring surface. Additional two phase-coherent, counter-propagating TM modes at wavelength λ_r are excited from either end of the bus waveguide to create an attractive optical lattice-like potential, localizing atoms tightly above the microring. Fig. 3 (d-e) plot the total trap potential U_{tot} , including the direct summation of repulsive and attractive potentials calculated using the electric field profiles obtained from the FEM analyses and the build-up intensity in the microring with a total input power of $P_b + 2P_r \approx 1.8 \text{ mW}$. We have also added in U_{tot} an approximate Casimir-Polder attractive potential $U_{\text{cp}} = -C_4/z(z^3 + \lambda^3)$, where $C_4 = h \times 267 \text{ Hz} \cdot \mu\text{m}^4$ is the Cs-Si₃N₄ surface interaction coefficient and $\lambda = 136 \text{ nm}$ is an effective wavelength³⁸.

The two-color evanescent field trap is robust and tunable. The vertical trap location z_t and the trap depth ΔU can be finely controlled by the power of injected light $P_{r(b)}$ (Fig. 3(f)). At an optimal power ratio shown in Fig. 3(e), the trap can be tuned to $z_t \approx 100 \text{ nm}$ with $\Delta U \approx k_B \times 120 \mu\text{K}$, much deeper than the thermal energy $\lesssim k_B \times 10 \mu\text{K}$ of polarization-gradient cooled cesium atoms, where k_B is the Boltzmann constant.

By realizing atom trapping and a critically-coupled microring resonator aligned to an atomic resonance, it is possible to probe the interaction between single atoms and resonator photons with high sensitivity. As a simple example, in Fig. 4 we plot a weakly-driven, steady-state bus waveguide transmission^{11,39}, $T(\delta) = \left| \frac{g^2 + (i\delta + \frac{\Gamma}{2})(i\delta + \frac{\kappa_1 + \kappa_c}{2})}{g^2 + (i\delta + \frac{\Gamma}{2})(i\delta + \frac{\kappa}{2})} \right|^2$, where

δ is the laser detuning from the atomic resonance (D2 line), $g = \sqrt{\frac{3\lambda_{D2}^3 \omega \Gamma}{16\pi^2 V_m}}$ is the position-dependent atom-photon coupling strength (Fig. 4(b) inset), $\Gamma = 2\pi \times 5.2 \text{ MHz}$ is the atomic decay rate, and the resonator decay rate $\kappa = \kappa_1 + \kappa_c = 2\pi \times 5.6 \text{ GHz}$ is extracted from the measurement. A trapped

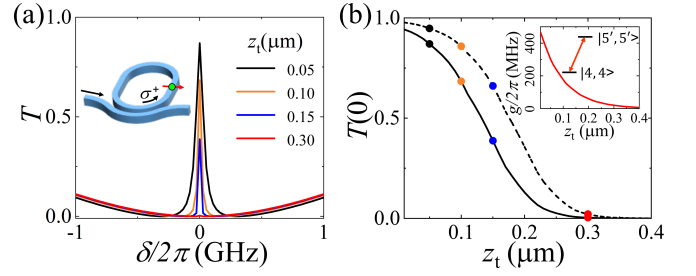


FIG. 4. (a) Transmission T with a spin-polarized atom trapped at the indicated positions z_t , calculated using $\kappa_c = \kappa_i = 2\pi \times 2.8 \text{ GHz}$ extracted from Fig. 3(c) and the atom-photon coupling strength g for σ^+ -transition driven by the CCW WGM as shown in the inset of (b). The polarization axis (red arrow) of the trapped atom (green sphere), and the CCW WGM (curved arrow) is depicted in the inset. (b) Resonant transmission $T(0)$ versus z_t (solid curve) and the case for $\kappa_c = \kappa_i = 2\pi \times 1.0 \text{ GHz}$ (dashed curve, for $Q \approx 3.3 \times 10^5$). Color symbols mark the trap locations as in (a).

atom is assumed to be initially polarized in the ground state $6S_{1/2}|F=4, m_F=4\rangle$ and is excited to $6P_{3/2}|F'=5, m_{F'}=5\rangle$ by a circularly polarized counter-clockwise (CCW) circulating WGM as shown in Fig. 4(a) inset. Significant increase in the bus waveguide transmission $T(0) \approx 1 - \kappa\Gamma/2g^2$ can be observed near the atomic resonance when $g^2 > \kappa\Gamma$. This transparency window results from the destructive interference between atom-WGM photon dressed states, similar to the electromagnetically-induced transparency effect^{40–42}. At the desired trap location $z_t \approx 100 \text{ nm}$, we expect $g \approx 2\pi \times 176 \text{ MHz}$ and $T(0) \approx 0.68$ ($T(0) \approx 0.86$ for currently best available $\kappa/2\pi \approx 2.0 \text{ GHz}$), which greatly contrasts $T(0) \approx 0$ of an empty microring (Fig. 4(b)). The large variation of bus waveguide transmission could thus inform us the presence of single atom and the strength of atom-photon coupling with high sensitivity^{39,43}. Lastly, we note that the WGM circular polarization results from strong confinement in the microring nanowaveguide; the polarization is locked to the direction of the WGM circulation⁴⁴. Creating a directional coupling with spin-polarized atoms can give rise to novel applications, for example, in chiral quantum optics^{4,6,45}.

We demonstrate a microring optical circuit that permits precision understanding of fabrication performance and analyses of the optical modes. Our circuit is efficiently coupled, scalable, and can simultaneously accommodate large number of atoms trapped in an array of surface micro traps. With near-term improvement on the membrane surface quality and reduction of other surface scattering sources, one expects more than ten-fold increase in Q/V_m than currently achieved values. Coherent quantum operations with a single atom or in a hybrid lattice formed by atoms and photons can be realized following introduction of cold atoms to the microring to form a hybrid quantum circuit with strong atom-photon interactions.

Funding is provided by the AFOSR YIP (Grant NO. FA9550-17-1-0298) and the ONR (Grant NO. N00014-17-1-2289). X. Zhou and M. Zhu acknowledge support from the Rolf Scharenberg Graduate Fellowship. The data that support the findings of this study are available from the corresponding

author upon reasonable request.

- ¹J. D. Thompson, T. G. Tiecke, N. P. de Leon, J. Feist, A. V. Akimov, M. Gullans, A. S. Zibrov, V. Vuletić, and M. D. Lukin, “Coupling a single trapped atom to a nanoscale optical cavity,” *Science* **340**, 1202–1205 (2013).
- ²T. G. Tiecke, J. D. Thompson, N. P. de Leon, L. R. Liu, V. Vuletić, and M. D. Lukin, “Nanophotonic quantum phase switch with a single atom,” *Nature* **508**, 241–244 (2014).
- ³A. Goban, C.-L. Hung, S.-P. Yu, J. D. Hood, J. A. Muniz, J. H. Lee, M. J. Martin, A. C. McClung, K. S. Choi, D. E. Chang, O. Painter, and H. J. Kimble, “Atom–light interactions in photonic crystals,” *Nature Communications* **5**, 3808 (2014).
- ⁴R. Mitsch, C. Sayrin, B. Albrecht, P. Schneeweiss, and A. Rauschenbeutel, “Quantum state-controlled directional spontaneous emission of photons into a nanophotonic waveguide,” *Nature Communications* **5**, 5713 (2014).
- ⁵A. Goban, C.-L. Hung, J. D. Hood, S.-P. Yu, J. A. Muniz, O. Painter, and H. J. Kimble, “Superradiance for atoms trapped along a photonic crystal waveguide,” *Phys. Rev. Lett.* **115**, 063601 (2015).
- ⁶M. Scheucher, A. Hilico, E. Will, J. Volz, and A. Rauschenbeutel, “Quantum optical circulator controlled by a single chirally coupled atom,” *Science* **354**, 1577–1580 (2016).
- ⁷N. V. Corzo, J. Raskop, A. Chandra, A. S. Sheremet, B. Gouraud, and J. Laurat, “Waveguide-coupled single collective excitation of atomic arrays,” *Nature* **566**, 359–362 (2019).
- ⁸P. Samutpraphoot, T. Đorđević, P. L. Ocola, H. Bernien, C. Senko, V. Vuletić, and M. D. Lukin, “Strong coupling of two individually controlled atoms via a nanophotonic cavity,” *Phys. Rev. Lett.* **124**, 063602 (2020).
- ⁹J. Perez-Rios, M. E. Kim, and C.-L. Hung, “Ultracold molecule assembly with photonic crystals,” *New Journal of Physics* **19**, 123035 (2017).
- ¹⁰S. Grandi, M. P. Nielsen, J. Cambiasso, S. Boissier, K. D. Major, C. Reardon, T. F. Krauss, R. F. Oulton, E. Hinds, and A. S. Clark, “Hybrid plasmonic waveguide coupling of photons from a single molecule,” *APL Photonics* **4**, 086101 (2019).
- ¹¹M. Zhu, Y.-C. Wei, and C.-L. Hung, “Resonator-assisted single molecule quantum state detection,” (2020), arXiv:2007.04498.
- ¹²J. D. Joannopoulos, S. G. Johnson, J. N. Winn, and R. D. Meade, *Photonic Crystals: Molding the Flow of Light (Second Edition)*, 2nd ed. (Princeton University Press).
- ¹³D. E. Chang, J. S. Douglas, A. González-Tudela, C.-L. Hung, and H. J. Kimble, “Colloquium: Quantum matter built from nanoscopic lattices of atoms and photons,” *Rev. Mod. Phys.* **90**, 031002 (2018).
- ¹⁴M. Hafezi, S. Mittal, J. Fan, A. Migdall, and J. Taylor, “Imaging topological edge states in silicon photonics,” *Nature Photonics* **7**, 1001–1005 (2013).
- ¹⁵T. Ozawa, H. M. Price, A. Amo, N. Goldman, M. Hafezi, L. Lu, M. C. Rechtsman, D. Schuster, J. Simon, O. Zilberberg, *et al.*, “Topological photonics,” *Reviews of Modern Physics* **91**, 015006 (2019).
- ¹⁶A. W. Elshaari, W. Pernice, K. Srinivasan, O. Benson, and V. Zwiller, “Hybrid integrated quantum photonic circuits,” *Nature Photonics* **1**, 1–14 (2020).
- ¹⁷L. Stern, B. Desiatov, I. Goykhman, and U. Levy, “Nanoscale light–matter interactions in atomic cladding waveguides,” *Nature communications* **4**, 1–7 (2013).
- ¹⁸P. Solano, P. Barberis-Blostein, F. K. Fatemi, L. A. Orozco, and S. L. Rolston, “Super-radiance reveals infinite-range dipole interactions through a nanofiber,” *Nature communications* **8**, 1–7 (2017).
- ¹⁹J. S. Douglas, H. Habibian, C.-L. Hung, A. V. Gorshkov, H. J. Kimble, and D. E. Chang, “Quantum many-body models with cold atoms coupled to photonic crystals,” *Nature Photonics* **9**, 326–331 (2015).
- ²⁰C.-L. Hung, A. González-Tudela, J. I. Cirac, and H. J. Kimble, “Quantum spin dynamics with pairwise-tunable, long-range interactions,” *Proceedings of the National Academy of Sciences* **113**, E4946–E4955 (2016).
- ²¹S.-P. Yu, J. D. Hood, J. A. Muniz, M. J. Martin, R. Norte, C.-L. Hung, S. M. Meenehan, J. D. Cohen, O. Painter, and H. J. Kimble, “Nanowire photonic crystal waveguides for single-atom trapping and strong light-matter interactions,” *Applied Physics Letters* **104**, 111103 (2014).
- ²²S.-P. Yu, J. A. Muniz, C.-L. Hung, and H. Kimble, “Two-dimensional photonic crystals for engineering atom–light interactions,” *Proceedings of the National Academy of Sciences* **116**, 12743–12751 (2019).
- ²³T.-H. Chang, B. M. Fields, M. E. Kim, and C.-L. Hung, “Microring resonators on a suspended membrane circuit for atom-light interactions,” *Optica* **6**, 1203–1210 (2019).
- ²⁴X. Luan, J.-B. Béguin, A. P. Burgers, Z. Qin, S.-P. Yu, and H. J. Kimble, “The integration of photonic crystal waveguides with atom arrays in optical tweezers,” *Advanced Quantum Technologies* , 2000008 (2020).
- ²⁵F. Le Kien, V. I. Balykin, and K. Hakuta, “Atom trap and waveguide using a two-color evanescent light field around a subwavelength-diameter optical fiber,” *Phys. Rev. A* **70**, 063403 (2004).
- ²⁶E. Vetsch, D. Reitz, G. Sagué, R. Schmidt, S. T. Dawkins, and A. Rauschenbeutel, “Optical interface created by laser-cooled atoms trapped in the evanescent field surrounding an optical nanofiber,” *Phys. Rev. Lett.* **104**, 203603 (2010).
- ²⁷A. Goban, K. S. Choi, D. J. Alton, D. Ding, C. Lacroûte, M. Pototschnig, T. Thiele, N. P. Stern, and H. J. Kimble, “Demonstration of a state-insensitive, compensated nanofiber trap,” *Phys. Rev. Lett.* **109**, 033603 (2012).
- ²⁸C.-L. Hung, S. M. Meenehan, D. E. Chang, O. Painter, and H. J. Kimble, “Trapped atoms in one-dimensional photonic crystals,” *New Journal of Physics* **15**, 083026 (2013).
- ²⁹M. E. Kim, T.-H. Chang, B. M. Fields, C.-A. Chen, and C.-L. Hung, “Trapping single atoms on a nanophotonic circuit with configurable tweezer lattices,” *Nature Communications* **10**, 1647 (2019).
- ³⁰C. Rossi, P. Temple-Boyer, and D. Estève, “Realization and performance of thin $\text{SiO}_2/\text{SiN}_x$ membrane for microheater applications,” *Sensors and Actuators A: Physical* **64**, 241–245 (1998).
- ³¹J. B. Béguin, J. Laurat, X. Luan, A. P. Burgers, Z. Qin, and H. J. Kimble, “Reduced volume and reflection for optical tweezers with radial laguerre-gauss beams,” (2020), arXiv:2001.11498 [quant-ph].
- ³²X. Ji, F. A. S. Barbosa, S. P. Roberts, A. Dutt, J. Cardenas, Y. Okawachi, A. Bryant, A. L. Gaeta, and M. Lipson, “Ultra-low-loss on-chip resonators with sub-milliwatt parametric oscillation threshold,” *Optica* **4**, 619–624 (2017).
- ³³J. Cardenas, C. B. Poitras, K. Luke, L. Luo, P. A. Morton, and M. Lipson, “High coupling efficiency etched facet tapers in silicon waveguides,” *IEEE Photonics Technology Letters* **26**, 2380–2382 (2014).
- ³⁴S. Woetzel, F. Talkenberg, T. Scholtes, R. Ijsselstein, V. Schultze, and H.-G. Meyer, “Lifetime improvement of micro-fabricated alkali vapor cells by atomic layer deposited wall coatings,” *Surface and Coatings Technology* **221**, 158–162 (2013).
- ³⁵E. R. Abraham and E. A. Cornell, “Teflon feedthrough for coupling optical fibers into ultrahigh vacuum systems,” *Applied optics* **37**, 1762–1763 (1998).
- ³⁶E. S. Hosseini, S. Yegnanarayanan, A. H. Atabaki, M. Soltani, and A. Adibi, “Systematic design and fabrication of high-q single-mode pulley-coupled planar silicon nitride microdisk resonators at visible wavelengths,” *Opt. Express* **18**, 2127–2136 (2010).
- ³⁷K. Srinivasan and O. Painter, “Mode coupling and cavity–quantum-dot interactions in a fiber-coupled microdisk cavity,” *Phys. Rev. A* **75**, 023814 (2007).
- ³⁸N. P. Stern, D. J. Alton, and H. J. Kimble, “Simulations of atomic trajectories near a dielectric surface,” *New Journal of Physics* **13**, 085004 (2011).
- ³⁹T. Aoki, B. Dayan, E. Wilcut, W. P. Bowen, A. S. Parkins, T. Kippenberg, K. Vahala, and H. Kimble, “Observation of strong coupling between one atom and a monolithic microresonator,” *Nature* **443**, 671–674 (2006).
- ⁴⁰C. Junge, D. O’Shea, J. Volz, and A. Rauschenbeutel, “Strong coupling between single atoms and nontransversal photons,” *Phys. Rev. Lett.* **110**, 213604 (2013).
- ⁴¹H. Tanji-Suzuki, W. Chen, R. Landig, J. Simon, and V. Vuletić, “Vacuum-induced transparency,” *Science* **333**, 1266–1269 (2011).
- ⁴²M. Mücke, E. Figueroa, J. Bochmann, C. Hahn, K. Murr, S. Ritter, C. J. Villas-Boas, and G. Rempe, “Electromagnetically induced transparency with single atoms in a cavity,” *Nature* **465**, 755–758 (2010).
- ⁴³I. Shomroni, S. Rosenblum, Y. Lovsky, O. Bechler, G. Guendelman, and B. Dayan, “All-optical routing of single photons by a one-atom switch controlled by a single photon,” *Science* **345**, 903–906 (2014).
- ⁴⁴T. V. Mechelen and Z. Jacob, “Universal spin-momentum locking of evanescent waves,” *Optica* **3**, 118–126 (2016).
- ⁴⁵P. Lodahl, S. Mahmoodian, S. Stobbe, A. Rauschenbeutel, P. Schneeweiss, J. Volz, H. Pichler, and P. Zoller, “Chiral quantum optics,” *Nature* **541**, 473–480 (2017).